Synthesis, structures, and catalytic studies of new copper(II) complexes with arene-linked pyrazolyl methane ligands

Ji-Xiao Wang, Xuan Wang, Ya-Nan Hou, Xiao-Dong Feng, Li-Xian Sun, Zhan Shi, Che Wang & Yong-Heng Xing

View supplementary material ↗

Submit your article to this journal ↗

Article views: 82

View related articles ↗

View Crossmark data ↗

Taylor & Francis
Taylor & Francis Group

Synthesis, structures, and catalytic studies of new copper(II) complexes with arene-linked pyrazolyl methane ligands

JI-XIAO WANG†, XUAN WANG†, YA-NAN HOU†, XIAO-DONG FENG†,
LI-XIAN SUN‡, ZHAN SHI§, CHE WANG*† and YONG-HENG XING*†

†College of Chemistry and Chemical Engineering, Liaoning Normal University, Dalian City,
PR China
‡Guangxi Key Laboratory of Information Materials, Guilin University of Electronic Technology,
Guilin, PR China
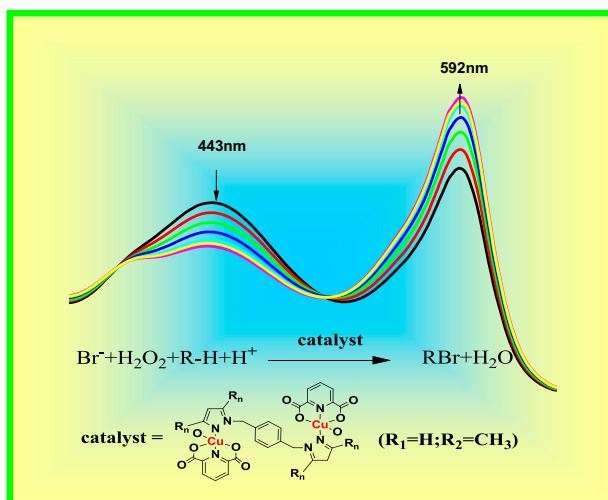§State Key Laboratory of Inorganic Synthesis and Preparative Chemistry, College of Chemistry,
Jilin University, Changchun, PR China

Two new copper complexes, $[Cu_2(L1)(dipic)_2(H_2O)_2]\cdot 2H_2O$ (**1**) and $[Cu_2(L2)(dipic)_2(H_2O)_2]\cdot 3H_2O$ (**2**) (L1 = 1,4-bis((1*H*-pyrazol-1-yl)methyl)benzene; L2 = 1,4-bis((3,5-dimethyl-1*H*-pyrazol-1-yl) methyl)benzene; and H_2dipic = 2,6-pyridinedicarboxylic acid), have been synthesized. The application of the copper complexes in bromination reaction was explored, and a mechanism was proposed.

Two new copper complexes, $[Cu_2(L1)(dipic)_2(H_2O)_2]\cdot 2H_2O$ (**1**) and $[Cu_2(L2)(dipic)_2(H_2O)_2]\cdot 3H_2O$ (**2**) (L1 = 1,4-bis((1*H*-pyrazol-1-yl)methyl)benzene; L2 = 1,4-bis((3,5-dimethyl-1*H*-pyrazol-1-yl) methyl)benzene; and H_2dipic = 2,6-pyridinedicarboxylic acid), were synthesized by the reaction of copper salt, arene-linked pyrazolyl methane ligands, and 2,6-pyridinedicarboxylic acid in 95% C_2H_5OH. They were characterized by elemental analysis, IR, UV–vis, single-crystal X-ray

---

*Corresponding authors. Email: wangche126@126.com (C. Wang); xingyongheng2000@163.com (Y.H. Xing)

diffraction analysis, X-ray powder diffraction, and thermogravimetric analysis. We explored the application of the copper complexes in bromination reactions; the complexes exhibited bromination catalytic activity in single-pot reaction for the conversion of phenol red into bromophenol blue. A feasible bromination reaction mechanism of copper complexes was proposed.

Keywords: Copper complexes; Arene-linked pyrazolyl methane; Hydrogen bond; Crystal structure; Oxidative bromination reaction

1. Introduction

There is interest in creating a variety of supramolecular coordination complexes which can be used as functional materials in crystal engineering, supramolecular chemistry, biochemistry, catalysis, materials science, sensors, separation techniques, etc. [1–11]. Ligand design has become a major concept in these investigations to tailor the stability and chemical properties of the complex [12]. Pyrazole and its derivatives are a crucial member of N-heterocyclic ligands, widely used in coordination chemistry due to their multiple nitrogens taking part in coordination with metals [13–15]. Pyrazole and its derivatives have high biological activities and widespread applications in pesticides and medicinal preparations [16–20]. Arene-linked pyrazolyl methane as third-generation bis(pyrazolyl) ligand has a rigid backbone and flexible bis(pyrazolyl) methane units [21, 22]. Multiple coordination sites of ligand can form structures of higher dimensions, and the high symmetry of ligands may result in new structures [23–25]. However, there are few investigations about complexes of arene-linked pyrazolyl methane with metals for applications in the field of bromoperoxidase mimicking as catalysts for oxidative bromination. The halogenated compounds are essential in organic chemistry as starting compounds, synthetic intermediates, and designer molecules for materials science, industrial chemicals, and bioactive compounds [26–28]. Enzymatic halogenation is an environmentally friendly route, but has not been commercialized on a large scale because of low operational stability of the haloperoxidase enzymes [29]. We found that a copper complex could be used in catalyzing oxidative bromination, the catalytic activity of which is similar to that of the bromoperoxidase [30]. For exploring new stable biomimetic catalysts and effect of different kinds of ligands on the catalytic activity, we have chosen two arene-linked pyrazolyl methanes as ligands, 1,4-bis((1*H*-pyrazol-1-yl)methyl)benzene (L1) and 1,4-bis((3,5-dimethyl-1*H*-pyrazol-1-yl)methyl)benzene (L2), to synthesize two new copper complexes, $[Cu_2(L1)(dipic)_2(H_2O)_2]\cdot 2H_2O$ (**1**) and $[Cu_2(L2)(dipic)_2(H_2O)_2]\cdot 3H_2O$ (**2**), and applied them in catalytic bromination. Herein, we report the synthesis, structure, and chemical properties of **1** and **2**. We explore the application in bromination of the copper complexes, and a feasible bromination reaction mechanism is proposed.

2. Experimental

2.1. *Materials and general procedure*

All the chemicals used were of analytical grade and used without purification. L1 (1,4-bis((1*H*-pyrazol-1-yl)methyl)benzene) and L2 (1,4-bis(3,5-dimethyl-1*H*-pyrazol-1-yl)methyl) benzene) were synthesized according to the literature method [31]. C, H, and N elemental analyses were carried out on a Perkin–Elmer 240C automatic analyzer. Infrared spectra were

recorded on a JASCO FT/IR-480 spectrometer with pressed KBr pellets from 4000 to 200 cm^{-1} and a Bruker AXS TENSOR-27 FT-IR spectrometer with KBr pellets from 4000 to 400 cm^{-1}. UV–vis spectra were recorded on a JASCO V−570 spectrometer (200–2500 nm, as a solid sample). The X-ray powder diffraction (PXRD) data were collected on a Bruker AXS D8 Advance diffractometer using Cu–Kα radiation (λ = 1.5418 Å) in the 2θ range of 5–60° with a step size of 0.02° and a scanning rate of 3°/min. Thermogravimetric analyses for the complexes were recorded on a Perkin–Elmer Diamond TG/DTA.

2.2. Synthesis of the complexes

2.2.1. Preparation of [Cu2(L1)(dipic)2(H2O)2] (1). L1 (0.024 g, 0.1 mmol) and Cu (CH$_3$COO)$_2$·2H$_2$O (0.020 g, 0.1 mmol) were mixed and stirred at room temperature for 1 h in a solution of 95% C$_2$H$_5$OH (10 mL). A solution of 2,6-pyridinedicarboxylic acid (H$_2$dipic) (0.033 g, 0.2 mmol) dissolved in the 95% C$_2$H$_5$OH (5 mL) was added dropwise to it, and then, the solution was stirred for 3 h at room temperature. The suspension was transferred into a Teflon-lined autoclave (20 mL) and kept at 100 °C for 3 days. The resulting solution was cooled down and filtered. After a few days, blue crystals of **1** were obtained, filtered off, and dried in air. Yield: 0.057 g, 75% (based on Cu(II)). Calcd for C$_{28}$H$_{28}$N$_6$O$_{12}$Cu$_2$: C, 43.91; H, 3.76; N, 10.69. Found: C, 43.77; H, 3.65; N, 10.89%.

2.2.2. Preparation of [Cu$_2$(L2) (dipic)$_2$(H$_2$O)$_2$]·3H$_2$O (2). Complex **2** can be obtained by similar procedures as **1**, but L2 (0.029 g, 0.1 mmol) was used instead of L1. After a few days, the blue crystals were obtained by filtering and washing with distilled water. Yield: 0.052 g, 62% (based on Cu(II)) Calcd for C$_{32}$H$_{38}$N$_6$O$_{13}$Cu$_2$: C, 44.89; H, 3.83; N, 9.85. Found: C, 45.11; H, 3.72; N, 9.79%.

2.3. X-ray single-crystal structural determinations

Suitable single crystals of **1** and **2** were mounted on glass fibers for X-ray measurement. Reflection data were collected at room temperature on a Bruker AXS SMART APEX II CCD diffractometer with graphite-monochromated Mo-Kα radiation (λ = 0.71073 Å) and a ω scan mode. All measured independent reflections ($I > 2\sigma(I)$) were used in the structural analyses, and semi-empirical absorption corrections were applied using SADABS [32]. The structures were solved by the direct method using SHELXL-97 [33]. All non-hydrogen atoms were refined anisotropically. Hydrogens of the organic frameworks were fixed at calculated positions geometrically and refined using a riding model. The hydrogens of the lattice water were found in the difference Fourier map. The crystallographic data and the structure refinement are given in table 1. Selected bond lengths and angles are listed in table 2.

2.4. Experimental setup for bromination reaction [30, 34–36]

Bromination activities were carried out in a mixed solution of H$_2$O-DMF at 30 ± 0.5 °C. The copper complexes (0.05 mmol) were dissolved in a 100 mL H$_2$O-DMF mixed solution with the volume ratio of 99:1. The solutions used for kinetic measurements were maintained at a constant concentration of H$^+$ (pH = 5.8) by the addition of NaH$_2$PO$_4$–Na$_2$HPO$_4$ buffer

Table 1. Crystallographic data for **1** and **2**.

Complexes	**1**	**2**
Formula	$C_{28}H_{28}N_6O_{12}Cu_2$	$C_{32}H_{38}N_6O_{13}Cu_2$
Molecular mass	767.64	841.78
Crystal system	Monoclinic	Triclinic
Space group	$P2_1/n$	$P\bar{1}$
a (Å)	11.222(3)	10.5339(8)
b (Å)	10.431(2)	11.2854(8)
c (Å)	13.706(3)	17.2399(12)
α (°)	90	101.9360(10)
β (°)	106.555(3)	93.9530(10)
γ (°)	90	114.5930(10)
V (Å^3)	1537.8(6)	1795.4(2)
Z	2	2
D_{calcd} (g cm^{-3})	1.658	1.557
Crystal size (mm)	0.38 × 0.28 × 0.20	0.32 × 0.31 × 0.22
$F(0\,0\,0)$	784	868
μ(Mo-Kα)/mm^{-1}	1.458	1.258
θ (°)	2.08–28.44	1.23–25.00
Reflections collected	9586	9040
Independent reflections [$I > 2\sigma(I)$]	3805(3406)	6278(4664)
Parameters	217	478
$\Delta(\rho)$ (e Å^{-3})	0.445, −0.635	1.263, −0.444
Goodness of fit	1.060	1.059
R[a]	0.0315(0.0355)[b]	0.0476(0.0723)[b]
wR_2[a]	0.0871(0.0902)[b]	0.1318(0.1449)[b]

[a]$R = \Sigma\|F_o| - |F_c\|/\Sigma|F_o|$, $wR_2 = \Sigma[w(F_o^2-F_c^2)^2]/\Sigma[w(F_o^2)^2c^{1/2}$; $[F_o > 4\sigma(F_o)]$.
[b]Based on all data.

Table 2. Selected bond lengths (Å) and angles (°) for **1** and **2**.

Cu–N(1)	1.8916(14)	Cu–N(2)	1.9519(16)	Cu–O(1)	2.0143(14)
Complex 1					
Cu–O(2)	2.0142(13)	Cu–O(5)	2.1492(14)		
N(1)–Cu–N(2)	157.53(6)	N(1)–Cu–O(1)	80.40(6)	N(1)–Cu–O(2)	80.65(6)
N(1)–Cu–O(5)	107.15(6)	N(2)–Cu–O(1)	97.24(6)	N(2)–Cu–O(2)	99.19(6)
N(2)–Cu–O(5)	95.29(6)	O(1)–Cu–O(2)	160.85(5)	O(1)–Cu–O(5)	94.11(5)
O(2)–Cu–O(5)	94.09(5)				
Complex 2					
Cu(1A)–N(1A)	1.914(3)	Cu(1A)–N(2A)	1.969(3)	Cu(1A)–O(1A)	2.055(3)
Cu(1A)–O(2A)	2.011(3)	Cu(1A)–O(5A)	2.252(3)	Cu(1B)–N(1B)	1.911(3)
Cu(1B)–N(2B)	1.962(4)	Cu(1B)–O(1B)	2.019(3)	Cu(1B)–O(2B)	2.027(3)
Cu(1B)–O(5B)	2.205(4)				
N(1A)–Cu(1A)–N(2A)	159.96(15)	N(1A)–Cu(1A)–O(1A)	79.57(13)	N(1A)–Cu(1A)–O(2A)	80.40(13)
N(1A)–Cu(1A)–O(5A)	94.74(13)	N(2A)–Cu(1A)–O(1A)	97.98(14)	N(2A)–Cu(1A)–O(2A)	99.73(13)
N(2A)–Cu(1A)–O(5A)	105.26(13)	O(1A)–Cu(1A)–O(2A)	159.71(12)	O(1A)–Cu(1A)–O(5A)	99.70(12)
O(2A)–Cu(1A)–O(5A)	85.13(12)	N(1B)–Cu(1B)–N(2B)	158.83(16)	N(1B)–Cu(1B)–O(1B)	80.61(14)
N(1B)–Cu(1B)–O(2B)	79.91(14)	N(2B)–Cu(1B)–O(1B)	100.48(15)	N(2B)–Cu(1B)–O(1B)	96.74(15)
N(2B)–Cu(1B)–O(2B)	99.57(14)	N(2B)–Cu(1B)–O(5B)	100.67(15)	O(1B)–Cu(1B)–O(2B)	159.86(13)
O(2B)–Cu(1B)–O(5B)	88.93(14)	O(1B)–Cu(1B)–O(5B)	99.62(15)		

solution. Reactions were initiated by the addition of phenol red solution. The copper complexes with six different concentrations were prepared in six cuvettes. Then, the cuvettes were put in constant temperature of water to heat for 5 min and spectral changes were recorded using a UV1000 spectrophotometer at 5-min intervals. Finally, the resulting data

were collected and fitted using the curve-fitting software in the program of Microsoft Excel. The rate constant of copper complexes in bromination reaction can be obtained according to the method of the literature [34, 35].

3. Results and discussion

3.1. *Synthesis*

Complexes **1** and **2** are synthesized by the reaction of copper salts, arene-linked pyrazolyl methane ligands (L1 and L2), and 2,6-pyridinedicarboxylic acid via hydrothermal reaction at 100 °C with the molar ratio of metal salt, ligands (L1 for **1**, L2 for **2**), and 2,6-pyridinedi-carboxylic acid equal to 1:1:2. To explore the factors affecting synthesis of **1** and **2**, we changed the adding sequence of the raw materials and the reaction temperature. It is found that: (1) When all raw materials are mixed and stirred simultaneously at room temperature and then using the hydrothermal method at 100 °C for 3 days, we get only Cu(dipic)$_2$ (scheme 1) instead of **1** and **2**. Obviously, the coordination ability of L1 and L2 is weaker than that of the 2,6-pyridinedicarboxylic acid. (2) The target complexes were tried to be synthesized by conventional solvent reaction method at room temperature but were unsuc-cessful. Through the results of these experiments, the adding sequence of raw materials and the reaction temperature are crucial factors for preparing the complexes.

3.2. *Structural description of 1 and 2*

3.2.1. [Cu2(L1)(dipic)2(H2O)2]·2H2O (1). Single-crystal X-ray diffraction analysis reveals that **1** crystallizes in the monoclinic, space group $P2_1/n$. The asymmetric unit of **1** contains one copper, a half of L1, one dipic, one coordinated water, and one lattice water as a distorted square pyramid [figure 1(a)]. Each Cu(II) is surrounded by two N and three O
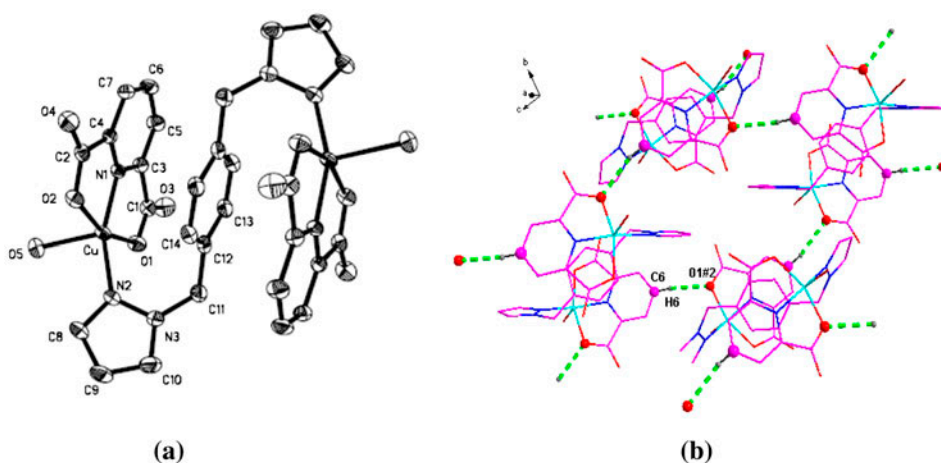

Figure 1. (a) Local coordination environment of Cu(II) in **1** (one lattice water is omitted for clarity); (b) a view of a 2D supermolecular network structure formed by hydrogen bonds C6-H6⋯O1$^{#2}$ (some hydrogens are omitted for clarity) (#2: $-1/2 + x$, $3/2 - y$, $-1/2 + z$).

atoms: N1, O1, O2 from a dipic, N2 from L1, and O5 from coordinated water. L1 links two Cu^{2+} ions by bidentate coordination with Cu⋯Cu distance of 7.1345(14) Å; the dipic adopts meridional tridentate chelating coordination. The bond distances of $Cu–N_{pz}$ and $Cu–N_{dipic}$ are 1.9519(16) and 1.8916(14) Å, respectively. The bond distances of $Cu–O_{dipic}$ and $Cu–O_{water}$ are 2.0142(13)–2.0143(14) Å and 2.1492(14) Å, respectively. The bond angle of N–Cu–N is 157.53(6)°, the angles of N–Cu–O are 80.40(6)°–107.15(6)°, and the angles of O–Cu–O are 94.09(5)°–160.85(5)°. The dihedral angle between benzene and pyrazole rings is 71.83(0.13)°, and the one between pyridine ring and pyrazole ring is 67.50(0.08)°.

There are three kinds of hydrogen bonds in the packing structure for **1** (table 3), including O5–H5⋯O4, C6–H6⋯O1, and C7–H7⋯O1W. The adjacent molecules are connected by the hydrogen bond C6–H6⋯O1$^{#2}$ [C6–H6⋯O1$^{#2}$, 3.246(2) Å, 160.7°, #2: $-1/2 + x$, $3/2 - y$, $-1/2 + z$] to form a 2D sheet structure [figure 1(b)]. Adjacent sheet structures are further connected by O5–H5⋯O4$^{#1}$ [O5–H5⋯O4$^{#1}$, 2.6867(19) Å, 160.0°, #1: $3/2 - x$, $-1/2 + y$, $1/2 - z$] to afford a 3D supermolecular network (figure S1, see online supplemental material at http://dx.doi.org/10.1080/00958972.2015.1028927). The hydrogen bonds enhance the stability of the molecular structure.

3.2.2. [Cu2(L2) (dipic)2(H2O)2].3H2O (2). Complex **2** crystallizes in the triclinic system with $P\bar{1}$ space group. X-ray single-crystal analysis indicates that the asymmetric unit of **2** consists of two Cu(II) ions, one L2, two dipic, two coordinated waters, and three lattice waters [figure 2(a)]. The Cu ions have the same coordination environment. The environment around each Cu can be described as a distorted square pyramid, coordinated by two nitrogens and three oxygens, N1, O1, and O2 from a dipic ligand, N2 from L2, and O5 from coordinated water. The coordination of L2 and dipic in **2** are similar to that in **1**, L2 links two Cu^{2+} ions (the distance of adjacent Cu ions is 7.1659(3) Å) by bidentate coordination and dipic adopts meridional tridentate coordination. The dihedral angles of benzene with pyrazole rings and pyridine with pyrazole rings are 74.97(0.46)° and 67.65(0.19)°, respectively. The bond distances of $Cu–N_{pz}$ are 1.969(3) and 1.962(4) Å, the distances of

Table 3. Hydrogen bond lengths (Å) and angles (°) of **1** and **2**.

D–H⋯A	d(D–H)/Å	d(H⋯A)/Å	d(D⋯A)/Å	∠D–H⋯A/°
Complex **1**				
O5–H5A⋯O4$^{#1}$	0.90	1.82	2.6867(19)	160.0
C6–H6⋯O1$^{#2}$	0.93	2.35	3.246(2)	160.7
C7–H7⋯O1W$^{#2}$	0.93	2.53	3.360(3)	148.8
Complex **2**				
O5A–H5A⋯O4B	0.90	2.05	2.829(5)	144.9
O5B–H5B⋯O4A	0.90	2.19	2.757(5)	120.1
O5B–H5C⋯O3W	0.90	1.95	2.841(6)	169.1
C15B–H15A⋯O5B	0.96	2.36	3.201(6)	145.8
O5A–H5B⋯O1A$^{#3}$	0.90	2.11	2.871(4)	142.0
C7A–H7A⋯O3B$^{#4}$	0.93	2.48	3.221(6)	136.3
C5B–H5⋯O4A$^{#4}$	0.93	2.44	3.289(6)	151.8
O3W–H3W⋯O1W$^{#5}$	0.85	2.33	2.888(6)	123.1
O3W–H3WA⋯O3B$^{#6}$	0.85	2.25	2.839(6)	126.6
O2W–H2WB⋯O3W$^{#6}$	0.85	1.98	2.805(9)	162.9
O1W–H1WB⋯O4B$^{#7}$	0.85	2.16	2.978(6)	160.9

Symmetry transformations used to generate equivalent atoms: #1: $3/2 - x$, $-1/2 + y$, $1/2 - z$; #2: $-1/2 + x$, $3/2 - y$, $-1/2 + z$; #3: $-x$, $-y$, $-z$; #4: $1 - x$, $1 - y$, $1 - z$; #5: $1 + x$, y, z; #6: $2 - x$, $1 - y$, $1 - z$; #7: x, $1 + y$, z.
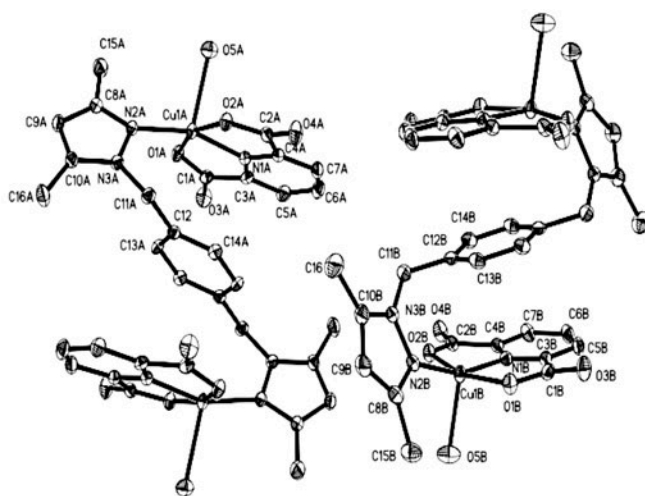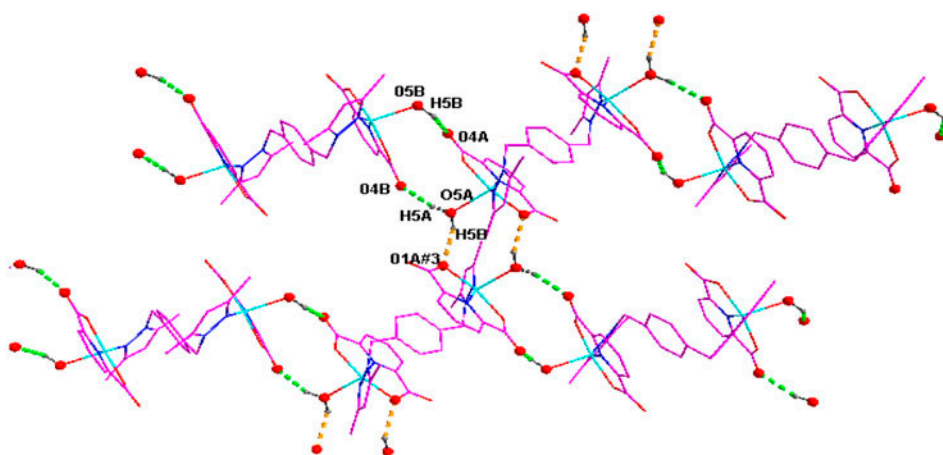
Figure 2. (a) Local coordination environment of Cu(II) in **2**; (b) an infinite helical chain structure of **2** by O5A–H5A···O4B and O5B–H5B···O4A hydrogen bonds; a view of a 2D supermolecular network structure formed by hydrogen bonds (some hydrogens are omitted for clarity) (#3: –x, –y, –z).

Cu–N$_{dipic}$ are 1.911(3) and 1.914(3) Å, the distances of Cu–O$_{water}$ are 2.205(4) and 2.252(3) Å, the distance of Cu–O$_{dipic}$ is 2.011(3)–2.055(3) Å. The bond angles of N–Cu–N are 158.83(16)° and 159.96(15)°, the angles of N–Cu–O and O–Cu–O are 79.57(13)°–105.26(13)° and 85.13(12)°–159.86(13)°, respectively. The bond lengths of **1** were slightly shorter than those of **2**, and the bond angles are close.

In the crystal packing structure of **2**, adjacent molecules are linked through hydrogen bonds of O5A–H5A···O4B and O5B–H5B···O4A [O5A–H5A···O4B, 2.829(5) Å, 144.9°; O5B–H5B···O4A, 2.757(5), 120.1°] to form an infinite chain. Adjacent chains are further linked by intermolecular weak interactions between O5A from coordinated water and O1A$^{#3}$ from dipic (O5A–H5B···O1A$^{#3}$, 2.871(4) Å, 142.0°, #3: –x, –y, –z) to afford a 2D

supermolecular network [figure 2(b)]. Adjacent sheet structures are further connected by O5B–H5C···O3W, C7A–H7A···O3B[#4], C5B–H5···O4A[#4], O3W–H3W···O1W[#5], O3W–H3WA···O3B[#6], and O1W–H1WB···O4B[#7] hydrogen bonds to form a 3D supermolecular network (O5B–H5C···O3W, 2.841(6) Å, 169.1°; C7A–H7A···O3B[#4], 3.221(6) Å, 136.3°; C5B–H5···O4A[#4], 3.289(6) Å, 151.8°, #4: $1 - x$, $1 - y$, $1 - z$; O3W–H3···O1W[#5], 2.888(6) Å, 123.1°, #5: $1 + x$, y, z; O3W–H3WA···O3B[#6], 2.839(6) Å, 126.6°, #6: $2 - x$, $1 - y$, $1 - z$; O1W–H1WB···O4B[#7]: 2.978(6) Å, 160.9°, #7: x, $1 + y$, z). All of these hydrogen bonds further enhance the stability of the molecular structure.

Comparing with related copper complexes, $\{[Cu(3,4-Hpdc)_2(H_2O)_2]\cdot 2dmso\}_n$ (3,4-H_2pdc = 3,4-pyridinedicarboxylic acid) and $Cu(2,5-pdc)(H_2O)_4\cdot H_2O$ (2,5-pdc = pyridine-2,5-dicarboxylate) [37, 38], the copper configuration, bond lengths, and angles between the copper ion and pyridinedicarboxylic acid were much different due to the positional isomers of pyridinedicarboxylic acid (table 4). The copper configurations in this work were described as the distorted square pyramidal geometry, but those of $\{[Cu(3,4-Hpdc)_2(H_2O)_2]\cdot 2dmso\}_n$ and $Cu(2,5-pdc)(H_2O)_4\cdot H_2O$ were octahedral. The order of $Cu–N_{pdc}$ bond lengths were 2,5-pdc > 3,4-pdc > 2,6-pdc, and the order of $Cu–O_{pdc}$ bond lengths were 2,5-pdc > 2,6-pdc > 3,4-pdc. The $N_{pdc}–Cu–O_{pdc}$ bond angles of the complexes with 2,5-pdc or 2,6-pdc as ligand were close due to coordinated N and O from the same pyridinedicarboxylic acid, and they were adjacent to each other.

3.3. *IR spectra*

The IR spectral data of **1** and **2** (figures S2 and S3) are listed in table S1. A broad absorption band at 3445 and 3423 cm^{-1} indicates the presence of water. Absorption at 3073–3100 cm^{-1} should be assigned to the stretch of =C–H from pyrazolyl ring, benzene ring, and pyridine ring. Bands at 2848–2968 cm^{-1} are the characteristic of C–H ($-CH_3$, $-CH_2$). Bands at 1665 and 1366 cm^{-1} for **1** and 1644 and 1364 cm^{-1} for **2** are attributed to the asymmetrical and symmetrical stretch of C=O, respectively. For **1**, peaks at 1630, 1518, and 1436 cm^{-1} are from C=C and C=N stretches of pyrazolyl ring, benzene ring, and pyridine ring. The bands at 1282 cm^{-1} are the characteristic of C–C or C–N. C–O band from dipic group is at 1184 cm^{-1}. The peak at 1077 cm^{-1} is N–N stretching vibration of pyrazolyl rings. IR spectral data of **2** are similar to that of **1**. Absorptions at 1554, 1466, 1427, 1297, 1270, 1180, and 1075 cm^{-1} are stretching vibrations of pyrazolyl and pyridyl rings.

3.4. *UV–vis absorption spectra*

The UV–vis absorption spectra of **1** and **2** (figure S4) are recorded as solid samples and their characteristic UV–vis bands are listed in table S2. Bands at 206 and 264 nm for **1** and

Table 4. Compared bond lengths (Å) and angles (°) for the copper complexes.

Complex	Cu–N$_{pdc}$	Cu–O$_{pdc}$	N$_{pdc}$–Cu–O$_{pdc}$	Ref.
1	1.8916(14)	2.0143(14), 2.0142(13)	80.40(16), 80.65(16)	This work
2	1.914(3), 1.911(3)	2.019(3), 2.011(3), 2.011(3), 2.027(3)	79.57(13), 80.61(14), 80.40(13), 79.91(14)	
3	2.006(2)	1.977(2)	89.77(10), 90.23(10)	[37]
4	2.072(4)	2.052(4)	79.46(16)	[38]

Notes: **3**: $\{[Cu(3,4-Hpdc)_2(H_2O)_2]\cdot 2dmso\}_n$; **4**: $Cu(2,5-pdc)(H_2O)_4\cdot H_2O$.

208 nm for **2** are attributed to π–π* transitions of the ligands. Bands at 307 and 338 nm for **1** and 272 and 339 nm for **2** are assigned to charge transfer transitions from the ligands to Cu(II) (*n*–π* transition) of N $\rightarrow$ Cu and O $\rightarrow$ Cu. Broad peaks at 765 nm for **1** and 788 nm for **2** could be caused by d $\rightarrow$ d* transition of Cu^{2+}, respectively.

3.5. *XRD analysis*

The composition of **1** amd **2** (figures S5 and S6) was confirmed by PXRD. It was used to confirm the phase purity of the bulk materials. The experimental results prove that all peaks presented in the measured patterns closely match the simulated patterns generated from single-crystal diffraction data.

3.6. *Thermal properties*

To examine the thermal stability of **1** and **2**, thermogravimetric analyses (TG) were carried out at a heating rate of 10 °C min^{-1} under nitrogen from 30 to 1000 °C (figures S7 and S8). In **1**, initial mass loss of 18.30% before 248 °C is due to the release of two lattice waters, two coordinated waters, and a pyrazole from L1 (Calcd 18.12%). The second mass loss of 55.40% from 248 to 307 °C is ascribed to the release of two dipic groups, one pyrazole molecular, and two -CH_2- groups from L1 (Calcd 55.12%). The last mass loss at 307–600 °C is ascribed to the release of the framework of the benzene ring of the L1, and the final residue corresponds to copper oxide. In **2**, the first mass loss of 10.50% is attributed to two lattice waters and three coordinated waters (Calcd 10.70%) from 30 to 125 °C. The second mass loss of 51.85% is attributed to release of two dipic groups, one 3,5-dimethyl pyrazolyl, and two -CH_2- groups from L2 (Calcd 52.18%) at 125–300 °C. The last step is from 300 to 1000 °C, considered to be the gradual decomposition of the framework of L2. The residues correspond to the copper oxide.

3.7. *Functional mimic of copper complexes*

3.7.1. Mimicking bromination reactions. Mimicking bromination reaction of copper complexes is similar to that of the oxidovanadium complexes [39–41]. The copper complexes mimic reaction in which copper species catalyze the bromination of organic substrates in the presence of H_2O_2 and bromide. Herein, the bromination activities of **1** and **2** using phenol red as an organic substrate are shown by the conversion of phenol red to bromophenol blue. The reaction is rapid and stoichiometric, producing the halogenated product by reaction of the oxidized halogen species with the organic substrate.

The addition of solution of **1** to the standard reaction of bromide in a phosphate buffer with phenol red as a trap for the oxidized bromine resulted in a visible color change of the solution from yellow to blue. As shown in figure 3, a decrease in the absorbance of the peak at 443 nm due to loss of phenol red and an increase in the absorbance of the peak at 592 nm characteristic of the bromophenol blue product are seen, showing that **1** possesses catalytic activities. The mimicking catalytic activities for **2** are similar to those of **1**.

3.7.2. Kinetic studies of the mimicking bromination reaction. Taking **1** as an example, a series of dA/dt data was obtained (figure 4) by changing the concentration of the copper complex. (The measurable absorbance dependence on time for **2** is shown in figure S9.)
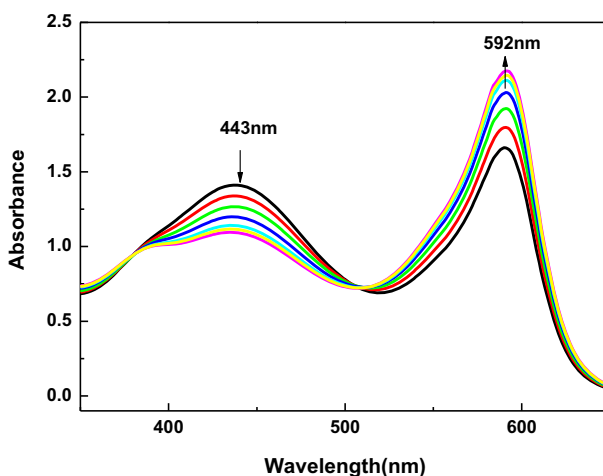
Figure 3. Oxidative bromination of phenol red catalyzed by **1**. Spectral changes at 10 min intervals. The reaction mixture contained a phosphate buffer (pH 5.8), KBr (0.4 mol L^{-1}), phenol red (10^{-4} mol L^{-1}), and **1** (0.51 × 10^{-5} mol L^{-1}).
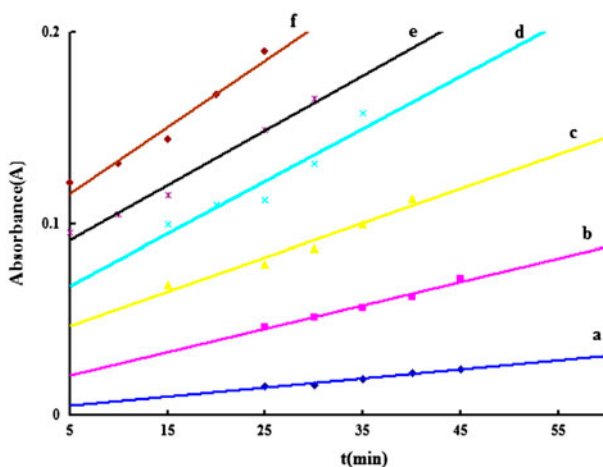

Figure 4. The measurable absorbance (592 nm) dependence on time for **1**. Conditions used: pH = 5.8, [KBr] = 0.4 mol L^{-1}, [H$_2$O$_2$] = 10^{-3} mol L^{-1}, [phenol red] = 10^{-4} mol L^{-1}. [complex **1**/mol L^{-1}] = a: 0.25 × 10^{-5}; b: 0.51 × 10^{-5}; c: 0.76 × 10^{-5}; d: 1.02 × 10^{-5}; e: 1.27 × 10^{-5}; f: 1.52 × 10^{-5}.

According to the data in figure 4, the plot of –log(dc/dt) *versus* –log c for **1** gave a straight line with a slope of 1.0898 and b = –1.3373, as shown in figure 5. The former confirmed that the reaction order is approximately first-order depending on copper. Based on the equation "b = log k + y log c_2 + z log c_3", the reaction rate constant, k, is determined by the concentrations of KBr and phenol red (c_2 and c_3), the reaction orders of KBr and phenol red (y and z), and b. In the experiment, considering that the reaction orders of KBr and phenol red (y and z) are one according to the literature [35, 36], c_2 and c_3 are 0.4 and 10^{-4} mol L^{-1}, respectively,

$$y = 1.0898x + 1.3373$$
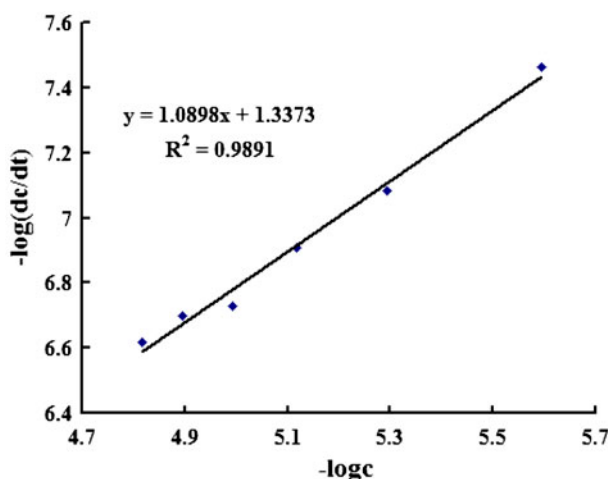$$R^2 = 0.9891$$

Figure 5. $-\log (dc/dt)$ dependence of $-\log c$ for **1** in DMF-H$_2$O at 30 ± 0.5 °C (c is the concentration of **1**); conditions used: pH = 5.8, [KBr] = 0.4 mol L^{-1}, [phenol red] = 10^{-4} mol L^{-1}.

so the reaction rate constant (k) for **1** can be calculated as 1.15×10^3 (mol L^{-1})$^{-2}$ s^{-1} ($-\log$ (dc/dt) dependence of $-\log c$ for **2** is shown in figure S10).

Plot for **2** was generated in similar way. The kinetic data in the system of DMF-H$_2$O at 30 ± 0.5 °C are shown in table 5. It is found that: (i) The reaction orders of the copper complexes in the bromination reaction are all close to 1, showing approximate first-order dependence on copper and (ii) the order of the reaction rate constant for them is **2 > 1**.

The catalytic bromination reaction mechanism is shown in scheme 2, in which, step a: the copper complex (CuLL′) is easy to form an intermediate [CuLL′O$_2$H] with H$_2$O$_2$ as an oxidation regent and in the condition of acidity (L: the ligand of L1 or L2; L′: dipic); step b: the intermediate species is transformed rapidly to copper radical species [CuL′O$_2$] and L (L1/L2); and step c: Br$^-$ is oxidized rapidly by [CuL′O$_2$], while at the same time, Br$^+$ and CuLL′ are formed. The catalytic reaction rate would be mainly based on the stability of the formed copper radical species [CuL′O$_2$] (step b). The experimental results show that the order of the catalytic activity is **2 > 1**. This is because the formation of the copper radical species [CuL′O$_2$] could be influenced by the electron density of the ligands and the bond length of Cu–N$_{pz}$. The catalytic activity of the complexes may correspond to different electron density of L1 and L2. There are four electron-donating –CH$_3$ groups which are conducive to forming copper radical species [CuL′O$_2$] with L2. L2 is easier to lose from the

Table 5. Kinetic data for the complexes in DMF-H$_2$O at 30 ± 0.5 °C.

Complex	X	b	k (mol L^{-1})$^{-2}$s^{-1}
1	1.0898	−1.3373	1.15×10^3
2	1.0843	−1.0025	2.49×10^3

Conditions used: [phosphate buffer] = 5×10^{-2} mol L^{-1}, pH = 5.8, [KBr] = 0.4 mol L^{-1}, [phenol red] = 10^{-4} mol L^{-1}, [H$_2$O$_2$] = 10^{-3} mol L^{-1}. X is the reaction order of the copper complex; b is the intercept of the line; k is the reaction rate constant for the copper complex.
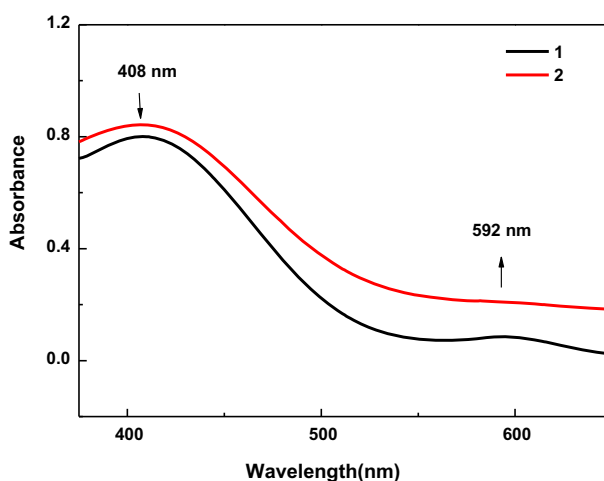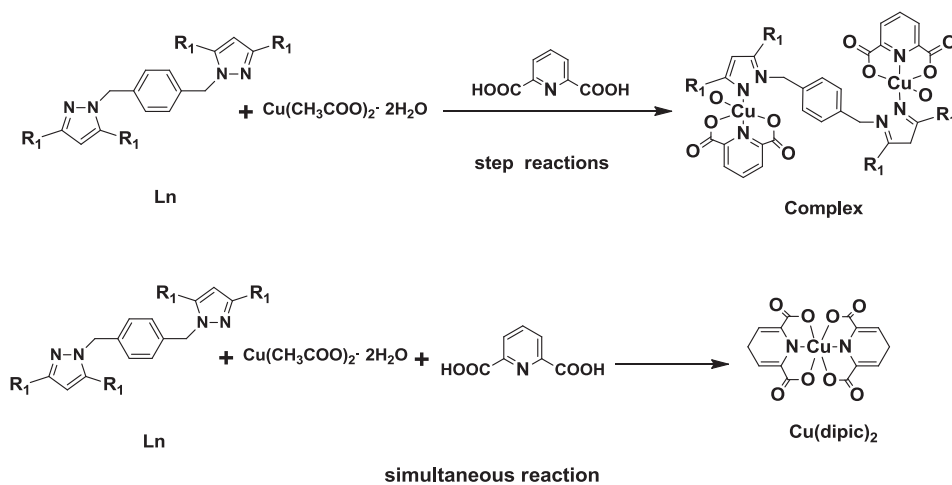
Figure 6. The bromophenol blue was changed by influence of **1** and **2** after 3 days. The reaction mixture contained a phosphate buffer (pH 5.8), KBr (0.4 mol L^{-1}), phenol red (10^{-4} mol L^{-1}), [**1**] = 0.51 × 10^{-5} mol L^{-1}, and [**2**] = 0.50 × 10^{-5} mol L^{-1}.

L1, Complex 1:R$_1$=H; L2, Complex 2 R$_1$= CH$_3$

Scheme 1. The synthetic routes of **1** and **2**.

complex than L1 due to the distance of Cu–N$_{pz}$ in **2** is slightly longer than that of **1**, also contributing to the catalytic activity order, **2 > 1**.

The color of bromination reaction during catalysis by the copper complex was changed slowly with time, and the blue color of bromophenol blue turned gradually light yellow. According to a large number of experimental studies, we thought bromophenol blue could be the intermediate species for oxidative bromination of phenol red and it would be
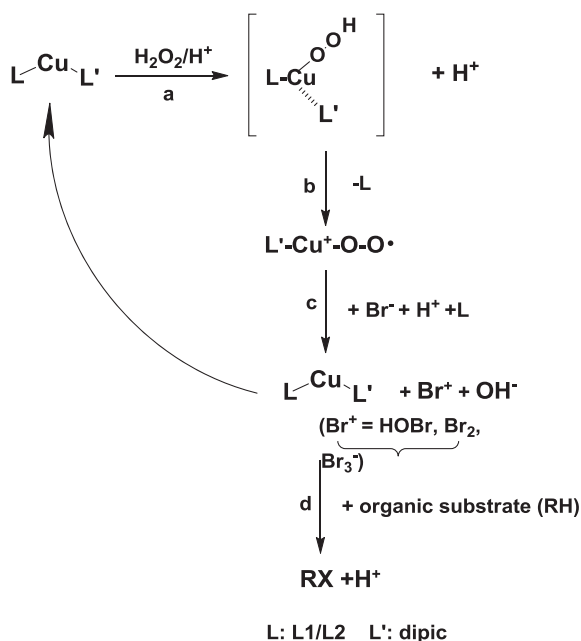
Scheme 2.   The catalytic bromination reaction mechanism for **1** and **2**.

degraded slowly into new species similar to phenol red as the experiment progressed. As shown in figure 6, the absorbance of the peak at 592 nm is characteristic of the bromophenol blue product decreases and the absorbance of the peak at 408 nm increases; composition of the new species is not clear. To explore the detailed mechanism further experiments are developing by our group.

4. Conclusion

Two copper complexes supported by N-heterocyclic ligands and 2,6-pyridinedicarboxylic acid are synthesized. Single-crystal X-ray diffraction analysis reveals that the copper ions are five-coordinate by N and O. The molecules of the complexes form various supramolecular structures via intermolecular hydrogen bonds. Adding sequence of raw materials and reaction temperature play a vital role in synthesizing compounds. The bromination reaction activities were tested with phenol red as substrate in the presence of H_2O_2, KBr, and phosphate buffer; **2** has a higher catalytic effect than **1**. Feasible bromination reaction mechanism is proposed.

Supplementary material

Tables of atomic coordinates, an isotropic thermal parameters, and complete bond distances and angles have been deposited with the Cambridge Crystallographic Data Center. Copies of this information may be obtained free of charge by quoting the publication

citation and deposition numbers CCDC: 1008980 for **1** and 1008979 for **2** from the Director, CCDC, 12 Union Road, Cambridge, CB2 1EZ, UK (Fax:+44–1223–336033; E-mail: deposit@ccdc.cam.ac.uk or http://www.ccdc.cam.ac.uk).

Disclosure statement

No potential conflict of interest was reported by the authors.

Funding

References

[1] Z. Wei, Z.-Y. Gu, R.K. Arvapally, Y.-P. Chen, R.N. McDougald Jr, J.F. Ivy, A.A. Yakovenko, D. Feng, M.A. Omary, H.-C. Zhou. *J. Am. Chem. Soc.*, **136**, 8269 (2014).
[2] C.K. Brozek, M. Dincă. *Chem. Sci.*, **3**, 2110 (2012).
[3] J. Zhang, Y. Zhang, J. Lin, X. Chen. *Chem. Rev.*, **112**, 1001 (2012).
[4] H.D. Clarke, K.K. Arora, H. Bass, P. Kavuru, T.T. Ong, T. Pujari, L. Wojtas, M.J. Zaworotko. *Cryst. Growth Des.*, **10**, 2152 (2010).
[5] C.B. Aakeroy, N.R. Champness, C. Janiak. *CrystEngComm.*, **12**, 22 (2010).
[6] J. An, N.L. Rosi. *J. Am. Chem. Soc.*, **132**, 5578 (2010).
[7] H. Li, B. Zhao, R. Ding, Y. Jia, H. Hou, Y. Fan. *Cryst. Growth. Des.*, **12**, 4170 (2012).
[8] Z. Hu, S. Pramanik, K. Tan, C. Zheng, W. Liu, X. Zhang, Y.J. Chabal, J. Li. *Cryst Growth Des.*, **13**, 4204 (2013).
[9] L. Zhang, L. Xu, X. Zhang, J. Wang, J. Li, Z. Chen. *Inorg. Chem.*, **52**, 5167 (2013).
[10] A.J. Nuñez, M.S. Chang, I.A. Ibarra, S.M. Humphrey. *Inorg. Chem.*, **53**, 282 (2014).
[11] F. Evangelisti, R. Güttinger, R. Moré, S. Luber, G.R. Patzke. *J. Am. Chem. Soc.*, **135**, 18734 (2013).
[12] A.L. Serrano, M.A. Casado, J.A. López, C. Tejel. *Inorg. Chem.*, **52**, 7593 (2013).
[13] X. Wang, Y.H. Xing, F.Y. Bai, X.Y. Wang, Q.L. Guan, Y.N. Hou, R. Zhang, Z. Shi. *RSC Adv.*, **3**, 16021 (2013).
[14] J. Manzur, C. Acuña, A. Vega, A.M. García. *Inorg. Chim. Acta*, **374**, 637 (2011).
[15] M.C. Carrion, I.M. Ortiz, F.A. Jalon, B.R. Manzano. *Cryst. Growth Des.*, **11**, 1766 (2011).
[16] A. Tanitame, Y. Oyamada, K. Ofuji, M. Fujimoto, N. Iwai, K. Hiyama, K. Suzuki, H. Ito, H. Terauchi, M. Kawasaki, K. Nagai, M. Wachi, J. Yamagishi. *J. Med. Chem.*, **47**, 3693 (2004).
[17] E.A. Musad, R. Mohamed, B.A. Saeed, B.S. Vishwanath, K.M. Lokanatha Rai. *Bioorg. Med. Chem. Lett.*, **21**, 3536 (2011).
[18] L. Xu, C. Zheng, L. Sun, J. Miao, H. Piao. *Eur. J. Med. Chem.*, **48**, 174 (2012).
[19] P. Lv, J. Sun, Y. Luo, Y. Yang, H. Zhu. *Bioorg. Med. Chem. Lett.*, **20**, 4657 (2010).
[20] (a) B.A. Thaher, M. Arnsmann, F. Totzke, J.E. Ehlert, M.H.G. Kubbutat, C. Schächtele, M.O. Zimmermann, P. Koch, F.M. Boeckler, S.A. Laufer. *J. Med. Chem.*, **55**, 961 (2012); (b) M. Grazul, E. Besic-Gyenge, C. Maake, M. Ciolkowski, M. Czyz, R.K.O. Sigel, E. Budzisz. *J. Inorg. Biochem.*, **135**, 68 (2014); (c) S. David, R.S. Perkins, F.R. Fronczek, S. Kasiri, S.S. Mandal, R.S. Srivastava. *J. Inorg. Biochem.*, **111**, 33 (2012); (d) M.E. López-Viseras, B. Fernández, S. Hilfiker, C.S. González, J.L. González, A.J. Calahorro, E. Colacio, A. Rodríguez-Diéguez. *J. Inorg. Biochem.*, **131**, 64 (2014); (e) R. Chen, C. Liu, H. Zhang, Y. Guo, X. Bu, M. Yang. *J. Inorg. Biochem.*, **101**, 412 (2007); (f) S. Gama, F. Mendes, F. Marques, I.C. Santos, M. Fernanda Carvalho, I. Correia, J.C. Pessoa, I. Santos, A. Paulo, *J. Inorg. Biochem.*, **105**, 637 (2011).
[21] S. Wang, G. Yuan, C. Sun, G. Yang, K. Shao, X. Wang, Y. Lan, Z. Su. *Inorg. Chem. Commun.*, **14**, 347 (2011).
[22] S. Wang, H. Zang, C. Sun, G. Xu, X. Wang, K. Shao, Y. Lan, Z. Su. *CrystEngComm.*, **12**, 3458 (2010).
[23] M. Broring, S. Prikhodovski. *Z. Anorg. Allg. Chem.*, **634**, 2451 (2008).
[24] I. Stein, U. Ruschewitz. *Z. Anorg. Allg. Chem.*, **635**, 914 (2009).
[25] C. Rohl. *Z. Anorg. Allg. Chem.*, **634**, 1633 (2008).

[26] S. Stavber, M. Jereb, M. Zupan. *Synthesis*, 1487, (2008).
[27] M.J. Dagani, H.J. Barda, T.J. Benya, D.C. Sanders. *Ullmann's Encyclopedia of Industrial Chemistry: Bromine Compounds*, Wiley-VCH, Weinheim (2002).
[28] J. Fauvarque. *Pure Appl. Chem.*, **68**, 1713 (1996).
[29] G. Grivani, V. Tahmasebi, A.D. Khalaji. *Polyhedron*, **68**, 144 (2014).
[30] D.X. Ren, N. Xing, H. Shan, C. Chen, Y.Z. Cao, Y.H. Xing. *Dalton Trans.*, **42**, 5379 (2013).
[31] X. Wang, S. Liu, C. Zhang, G. Song, F. Bai, Y. Xing, Z. Shi. *Polyhedron*, **47**, 151 (2012).
[32] G.M. Sheldrick. *SADABS, Program for Empirical Absorption Correction for Area Detector Data*, University of Göttingen, Göttingen (1996).
[33] G.M. Sheldrick. *SHELX-97, Program for Crystal Structure Analysis*, University of Göttingen, Göttingen (1997).
[34] C. Chen, Q. Sun, D. Ren, R. Zhang, F. Bai, Y. Xing, Z. Shi. *CrystEngComm.*, **15**, 5561 (2013).
[35] T.N. Mandal, S. Roy, A.K. Barik, S. Gupta, R.J. Butcher, S.K. Kar. *Polyhedron*, **27**, 3267 (2008).
[36] A. Pohlmann, S. Nica, T.K.K. Luong, W. Plass. *Inorg. Chem. Commun.*, **8**, 289 (2005).
[37] F.M. Scaldini, C.C. Corrêa, M.I. Yoshida, K. Krambrock, F.C. Machado. *J. Coord. Chem.*, **67**, 2967 (2014).
[38] S. Manna, S. Mistri, E. Zangrando, S.C. Manna. *J. Coord. Chem.*, **67**, 1174 (2014).
[39] R.I. Rosa, M.J. Clague, A. Butler. *J. Am. Chem. Soc.*, **114**, 760 (1992).
[40] M.R. Maurya, S. Agarwal, C. Bader, M. Ebel, D. Rehder. *Dalton Trans.*, 537, (2005).
[41] M.R. Maurya, A. Kumar, M. Ebel, D. Rehder. *Inorg. Chem.*, **45**, 5924 (2006).